Highly Efficient Restoration of Graphitic Structure in Graphene Oxide Using Alcohol Vapors

Ching-Yuan Su,[†,¶] Yanping Xu,[‡,¶] Wenjing Zhang,[‡] Jianwen Zhao,[‡] Aiping Liu,[§] Xiaohong Tang,[⊥] Chuen-Horng Tsai,[∥] Yizhong Huang,[‡] and Lain-Jong Li[†,*]

[†]Research Center for Applied Sciences, Academia Sinica, Taipei 11529, Taiwan, [‡]School of Materials Science and Engineering, Nanyang Technological University, Singapore 637819, [§]School of Mechanical and Aerospace Engineering, Nanyang Technological University, Singapore 639798, [⊥]Photonics Research Centre, Microelectronics Division, School of Electrical and Electronic Engineering, Nanyang Technological University, Singapore 639798, and [∥]Department of Engineering and System Science, National Tsing Hua University, Taiwan 30013. [¶]These authors contributed equally to this work.

ABSTRACT Solution-based processes involving the chemical oxidation of graphite and reduction of the obtained graphene oxide (GO) sheets have attracted much attention for preparing graphene films for printed electronics and biosensors. However, the low electrical conductivity of reduced GO is still hindering the development of electronic applications. This article presents that GO sheets reduced by high-temperature alcohol vapors exhibit highly graphitic structures and excellent electrical conductivity. The sheet resistance of thin transparent films is lowered to ~15 kΩ/□ (>96% transparency). Field-effect transistors produced from these reduced GO sheets exhibit high effective field-effect hole mobility up to 210 $cm^2/V \cdot s$. Raman spectroscopic studies reveal that the conductivity enhancement in the low mobility regime is attributed to the removal of chemical functional groups and the formation of six-fold rings. In the high mobility regime, the growth of the graphitic domain size becomes dominant for enhancing its electrical conductivity. The excellent electrical conductivity of the reduced GO sheets promises potential electronic applications.

KEYWORDS: graphene oxide · Raman spectroscopy · transistors · transparent conducting electrodes

Since the discovery of single-layer graphene (SLG),[1−3] it has attracted intensive interest due to its two-dimensionality and unique physical properties such as high intrinsic carrier mobility (~200 000 $cm^2/V \cdot s$),[4] quantum electronic transport,[2,5] tunable band gap,[6,7] high mechanical strength and elasticity,[8] and superior thermal conductivity.[9] These outstanding properties make graphene promising for high-speed transistor applications,[10−14] transparent conductive thin films,[14−17] reinforced composites,[18] and energy storage.[19] Moreover, graphene-based field-effect transistors for biological sensors[20−23] have recently attracted much attention since the electrical property of graphene is highly sensitive to its local environment. In addition to mechanical exfoliation,[1] epitaxial growth,[24−26] and chemical vapor deposition (CVD),[27,28] the chemical, thermal, or photocatalytic reduction of graphene oxide (GO) has been recently considered as a potential method for producing SLG sheets.[14,29−34] The exfoliated single-layer GO sheets can be well-dispersed in aqueous solutions, potentially useful for making graphene patterns with lithography-free processes such as inkjet or transfer printing. In addition, the solution-compatible process has potential in large-area, scalable, and cost-effective electronics. According to the commonly used Hummers' method,[35] graphite powders are treated with oxidation for adding oxygen-containing functional groups on the edges and basal planes of graphite flakes. These functional groups then reduce the interplanar forces, promoting complete exfoliation to single-layer GO sheets in aqueous media. Here, the modified Hummers' method, where a sonication process was added to better adjust the size of the obtained GO sheets, was used to prepare large-size single-layer GO sheets.[36] Using these large-size (>20 μm in lateral size) monolayered GO sheets, transparent electrodes and field-effect transistors can be easily fabricated. This enables detailed studies of the graphitic structure−electrical property relationship. There have been reports on the reduction of GO into graphene using chemical routes[29,33,37−40] and thermal annealing.[16,39−44] The reduction processes of GO sheets still can be improved and require systematic investigation particularly in the graphitic structure−electrical property relationship. It is discovered that alcohol vapors are more effective in the reduction of GO sheets in contrast to the commonly used high-temperature annealing with H_2. Such a simple and efficient process allows us to obtain highly conductive transparent

*Address correspondence to lanceli@gate.sinica.edu.tw.

Received for review July 19, 2010 and accepted August 13, 2010.

Published online August 18, 2010.
10.1021/nn101691m

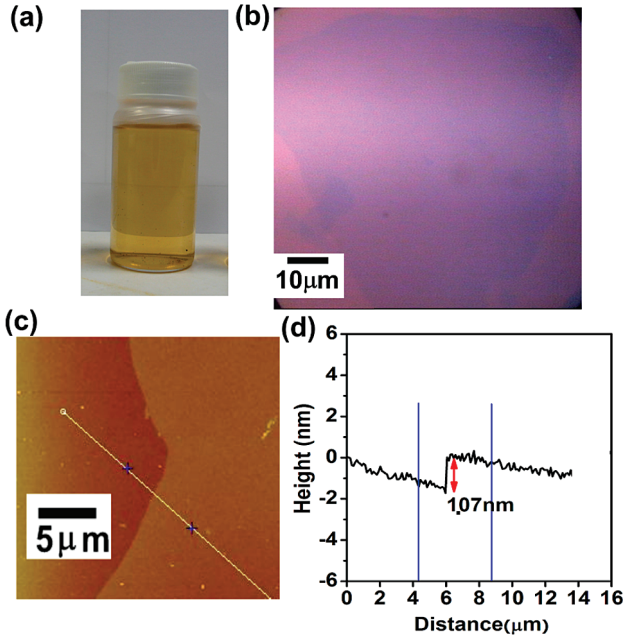

Figure 1. (a) As-prepared GO solution. (b) Optical image for a single-layer GO sheet (on 300 nm SiO_2) produced by the modified method (with 2 h sonication). (c) Corresponding AFM image and (d) AFM height profile for the GO sheet. AFM measurement along the white solid line in (c) shows that the sheet is ~1 nm thick.

electrodes (sheet resistance ~15 kΩ/□; 96% transparency at 550 nm). The field-effect transistors produced from these alcohol-reduced GO sheets also exhibit high effective hole mobility up to 210 $cm^2/V \cdot s$. Recently, Gao *et al.* elucidated the reduction processes of GO using synthetic chemistry,[41] and the restoration of conductivity was explained by the removal of functionalities. Here, it is shown that low-temperature alcohol vapor reduction (600 °C) is already capable of removing most of the oxygen-containing functionalities. However, at higher temperature (>800 °C) reduction, the enhancement in the domain size of nanographitic

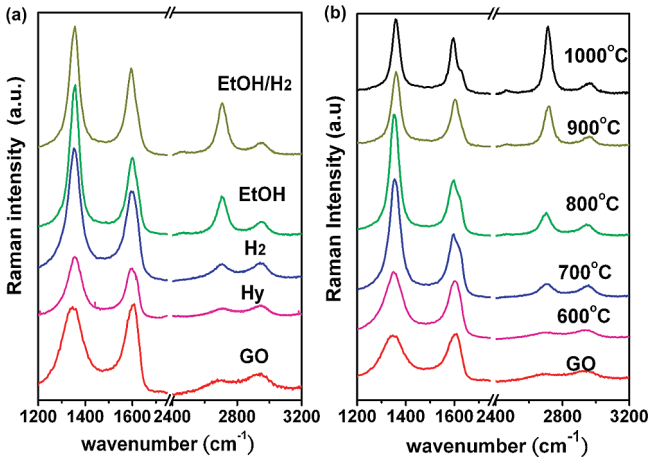

Figure 2. (a) Raman spectra for monolayered GO sheets before and after various reduction procedures including hydrazine vapor soaking (Hy), H_2 annealing (900 °C; 20% H_2 in Ar), alcohol reduction (at 900 °C; Ar as a carrier gas), and alcohol/H_2 reduction (900 °C; 20% H_2/Ar as a carrier gas). (b) Raman spectra for the GO sheets after alcohol reduction at 600, 700, 800, 900, and 1000 °C.

structures is the major cause for recovering their electrical conductivity.

RESULTS AND DISCUSSION

Preparation of Large Graphene Oxide Sheets. Since the 19th century, graphite oxide has been produced by Hummers' method,[14,29,35,44] which typically involves oxidation of graphite in the presence of strong oxidants and acids for extended periods. Here, we modified the Hummers' method as reported by Xu *et al.*,[45] where we replace the first step (the chemical oxidation of graphite flakes using concentrated H_2SO_4, P_2O_5, and $K_2S_2O_8$) with a sonication process in concentrated H_2SO_4 to break graphite flakes into the flakes with the desired size as discussed elsewhere.[36] The subsequent oxidation process allows us to obtain fairly large size (>20 μm in lateral size) of GO sheets, which is useful for preparing devices for electrical measurements. Figure 1a shows the photo of the solution containing ultralarge GO sheets produced from the modified method with 2 h sonication. Figure 1b displays the typical optical image for a single-layer GO sheet dip-coated on a 300 nm SiO_2/Si substrate, where the lateral size of the GO sheets typically ranges from 20 to 100 μm. Figure 1c,d shows the AFM image and its height profile for the obtained GO sheet. The measured thickness for the GO sheet was ~1.07 nm, suggesting that it was a single-layer GO sheet.

Reduction of Graphene Oxides Using Alcohol Vapors. Alcohols have been used as the carbon feedstock to synthesize high-purity single-walled carbon nanotubes at high temperatures (550−900 °C) in the presence of catalytic particles.[46] The OH radicals dissociated from alcohol molecules are able to attack carbon atoms with a dangling bond, leaving single-walled carbon nanotubes (SWNTs) to survive in the reaction conditions.[46] Here, instead of growing SWNTs, the alcohol reduction process is adopted to reduce the GO sheets. Figure 2a shows the Raman spectra for monolayered GO sheets before and after various reduction procedures, including hydrazine vapor soaking (Hy), H_2 annealing (900 °C; 20% H_2 in Ar), alcohol reduction (at 900 °C; Ar as a carrier gas), and alcohol/H_2 reduction (900 °C; 20% H_2/Ar as a carrier gas). The well-known *G* peak (at ~1585 cm^{-1}) and 2D peak (at ~2700 cm^{-1}) are characteristic of the sp^2-hybridized carbon−carbon bonds in graphene.[47−50] It is noted that the ratio of *the integrated Raman peak area* between the 2D and G bands, *I*(2D)/*I*(G), has been shown to be related to the degree of recovery for sp^2 C═C bonds (graphitization) in graphitic structures.[50] Figure 2a clearly shows that the *I*(2D)/*I*(G) after reduction using alcohol vapors with or without introducing H_2 gas is much higher than that with H_2 annealing or hydrazine reduction. This observation demonstrates that the high efficiency of restoring sp^2 carbon is strongly related to the presence of alcohol vapors. Nevertheless, the reduction using pure alcohol

TABLE 1. Comparison of Ultrathin Electrodes Prepared from Various Reduced GO Sheets

sample ID	process	transparency (% @550 nm)	sheet resistance (kΩ/□)
1	20%H_2/Ar with alcohol, 900 °C, 30 min	98.2	43
2	20%H_2/Ar, 900 °C, 2 h	98.1	413
3	20%H_2/Ar with alcohol, 1000 °C, 30 min	96.2	15
4	20%H_2/Ar, 1000 °C, 2 h	98.0	188
5[a]	1100 °C vacuum annealing, 3 h	95.0	500
6[b]	hydrazine reduction	95.4	19000

[a]From ref 42. [b]From ref 37.

vapor will produce some amorphous carbons due to the recombination of excess carbon radicals decomposed from alcohol. Therefore, introducing small amounts of H_2 flow during the reduction process is helpful to keep the process clean (by suppressing the formation of amorphous carbon). It is noticed that from Raman measurement there is no sign of forming amorphous carbon on GO film if 20% H_2/Ar is used as a carrier gas in alcohol reduction (Raman spectra in Supporting Information Figure S1 and AFM images in Figure S2 show that amorphous carbon can sometimes be observed on GO if no H_2 gas is supplied during the reduction). The absence of amorphous carbon is also verified by another control experiment, where the reduction with 20% H_2/Ar with alcohol does not produce amorphous carbon on HOPG from Raman analysis (Figure S3). Therefore, in the subsequent alcohol reduction processes 20% H_2/Ar is used to carry alcohol vapor for performing the reduction for GO sheets. Figure 2b compares the Raman spectra for the GO sheets after alcohol reduction at 600, 700, 800, 900, and 1000 °C. The 2D band emerges at 700 °C and becomes more pronounced at 900 and 1000 °C. The ratio $I(2D)/I(G)$ even reaches a value >1.4 at 1000 °C reduction. The temperature study suggests that high-temperature (900−1000 °C) alcohol reduction is able to achieve efficient restoration of graphitic structure in GO. In addition, the AFM measurements show that the thickness of the monolayered GO sheet after reduction is kept unchanged.

Electrical Properties of Alcohol-Reduced GO Films. To confirm the restoration of graphitic structures in GO films by alcohol reduction, transparent thin films based on the GO sheets reduced at various temperatures were deposited onto quartz substrates using the dip-coating method. Figure S4 (Supporting Information) shows the scanning electron microscope images for the assembled reduced GO films. Table 1 shows that the sheet resistance of the GO transparent electrodes decreases from ~43 kΩ/□ (900 °C reduction with alcohol) to ~15 kΩ/□ (1000 °C reduction with alcohol), where the thin films have similar transparency (T = 96−98%, corresponding to 1 or 2 layer GO). Since the absorption of a single-layer graphene in the visible range is ~2.7%,

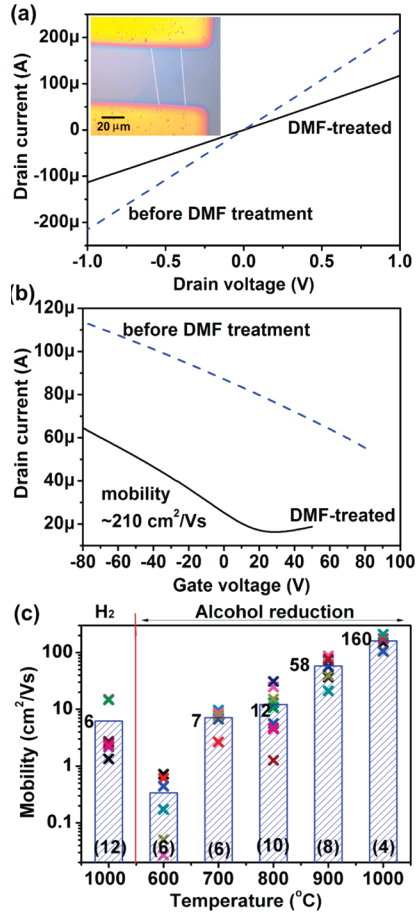

Figure 3. (a) Typical output characteristics (drain current I_d *vs* drain voltage V_d) and (b) transfer curves for a single-layer GO sheet after 1000 °C alcohol reduction with or without DMF treatment. (c) Statistical mobility data for the devices made from monolayered GO sheets reduced at various temperatures.

the slight deviation of absorption obtained may come from the discontinuous coverage of GO sheets. For comparison, the GO thin films after reduction without alcohol exhibit significantly higher sheet resistance (188−413 kΩ/□). It is noted that the sheet resistance for the alcohol-reduced GO electrodes at a lower temperature 900 °C, ~42 kΩ/□ (T ~ 98%), is already comparable with the 40−100 kΩ/□ (T ~ 95%) obtained by vacuum annealing at 1100 °C.[42] The typical sheet resistance for hydrazine-reduced GO electrodes[37] is also listed in the table for comparison. These results suggest that alcohol vapor-assisted reduction is highly efficient in enhancing the conductivity of GO.

In addition, bottom-gate-operated transistors were fabricated by evaporating Au electrodes directly on top of the reduced GO sheets, which were previously deposited on SiO_2/Si substrates. Figure 3a demonstrates the typical output characteristics (drain current I_d *vs* drain voltage V_d) for the device prepared from a single-layer GO sheet after 1000 °C alcohol reduction. Inset shows the photograph of the device, where the graphene edge is indicated by dotted lines. Only GO

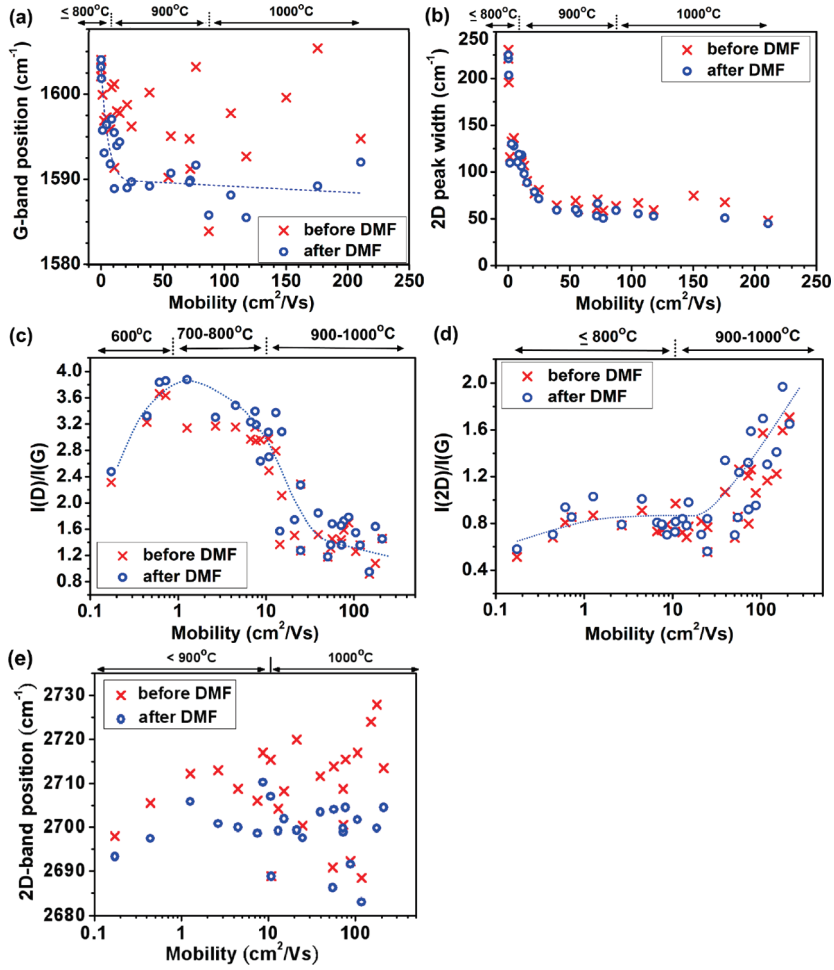

Figure 4. Correlations of (a) G band position, (b) 2D peak width, (c) integrated peak intensity ratio of *I*(D)/*I*(G), (d) integrated peak ratio of *I*(2D)/*I*(G) and, (e) 2D frequency with the field-effect mobility.

sheets with regular shapes and suitable sizes were used for transistor fabrications because it is convenient to extract their field-effect carrier mobility. Figure 3b shows the transfer curves (I_d *vs* gate voltage V_g) for the device. No neutrality point (Dirac point) is observed for the as-prepared device within V_g scanning range, likely because the reduced GO sheet is still heavily p-doped. The Dirac point of the device can be shifted back to 0−30 V once the device is soaked with DMF vapors for 8 h, where the DMF dopes the device with electrons and left-shifts the Dirac point. In addition, it is reasonable that the I_d is consequently reduced, as shown in Figure 3a, due to the decrease in the hole carrier concentration. The transfer curves for several other high mobility devices are provided in Supporting Information Figure S5. The field-effect mobility of holes was extracted based on the slope $\Delta I_d/\Delta V_g$ fitted to the linear regime of the transfer curves using the equation $\mu = (L/WC_{ox}V_d)(\Delta I_d/\Delta V_g)$, where L and W are the channel length and width and C_{ox} the gate capacitance. The field-effect mobility of the alcohol-reduced GO sheets goes up to ~210 $cm^2/V \cdot s$ in ambient condition, which is at least 2 orders of magnitude higher than the reported ~0.1−1 $cm^2/V \cdot s$ after hydrazine chemical reduction.[33] Figure 3c compiles the mobility data for the devices made from monolayered GO sheets reduced at various temperatures, where the number in parentheses indicates the number of devices prepared. The statistical results clearly demonstrate that the mobility increases with a reduction in temperature, consistent with the Raman results in Figure 2b. Moreover, the device mobility for the GO sheet reduced from H_2 gas at 1000 °C is much lower than those from alcohol reduction at the same temperature, consistent with the conclusion from Raman studies (Figure 2a).

Correlation between Spectroscopic Results and Electrical Properties. To correlate the electrical properties of the single-layer GO sheets with their structural changes, confocal Raman spectroscopy was adopted to directly characterize the reduced GO sheets in transistor devices with effective field-effect mobility values from 0.05 to 210 $cm^2/V \cdot s$. The mobility values were extracted only after DMF soaking; therefore, they were used as the indices for the degree of graphitic structure restoration. The correlations of several Raman features (G band position, 2D peak posi-

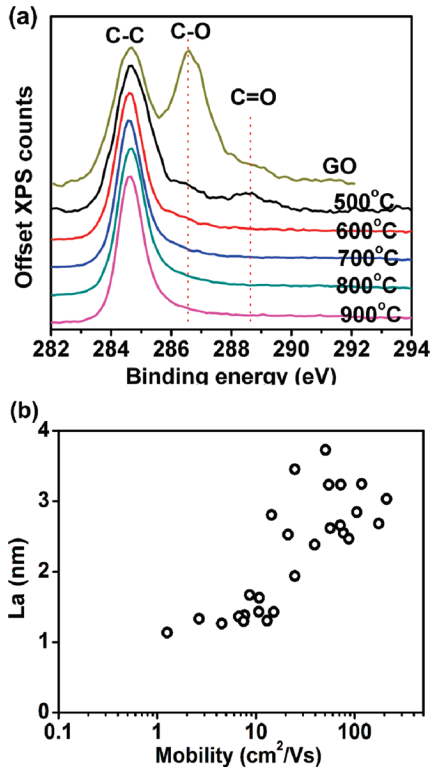

Figure 5. (a) XPS characterizations for the GO sheets reduced at various temperatures as indicated. (b) Estimated graphene nanocrystallite size increases with the mobility.

tion, 2D peak width and integrated peak ratio of I(D)/I(G) and I(2D)/I(G)) and the field-effect mobility are shown in Figure 4, where the Raman data before DMF soaking were also included for comparison. In general, the Dirac point of each device is shifted toward 0 V after DMF soaking, and the p-doping effect is reduced. The trend of n-doping of reduced GO by DMF is also confirmed by the left-shift of Raman 2D frequency[51] after DMF soaking, as shown in Figure 4e. Hence, the relation between Raman signatures and carrier mobilities in Figure 4 is more informative because both sets of data (before and after DMF soaking) are included. All Raman peaks including G, D, D′, 2D, and other high-energy overtune bands in each spectrum were fitted with a Lorentzian function (see Supporting Information Figure S6 for an example). Figure 4a demonstrates that the peak position of the G band of GO sheets initially at around 1600 cm^{-1} is clearly downshifted to 1590 cm^{-1} with the increase of mobility in the early stage (from ~0.05 up to 10 $cm^2/V \cdot s$, corresponding to the reduction performed at ≤800 °C). It has been concluded that the downshift of G band frequency in graphite corresponds to the development of long-range in-plane order or establishment of a three-dimensional graphite structure.[52,53] At this stage, the chemical functional groups are being removed and six-fold graphitic rings built. XPS characterizations shown in Figure 5a suggest that the removal of the majority of chemical functional groups (oxygen containing species such as C−O and C═O) occurs even at a lower temperature regime (<600 °C). With further increase in device mobility (from 10 up to 210 $cm^2/V \cdot s$, corresponding to the temperature ≥800 °C), the G band frequency approaches 1590 cm^{-1} and becomes less sensitive to the mobility. The less sensitive and lower G band frequency corresponds well to the restoration of the graphitic structure in GO, and similar observations for graphite have been reported.[52] This suggests that at higher temperature the growth of graphitic nanodomains becomes the dominant process rather than the removal of chemical functional groups.[36] Moreover, the 2D band located at ~2700 cm^{-1}, the second-order Raman feature of the D band, originates from a double-resonance process.[50,53−55] The decrease of the 2D peak width has been used to indicate the restoration of graphitic structures in graphite.[52] Figure 4b shows that the 2D peak width decreases rapidly with mobility in the low mobility regime and approaches 50 cm^{-1} in the high mobility regime, corresponding well to the evolution of the G band frequency in Figure 4a.

Examining the evolution of I(D)/I(G) with mobility (as shown in Figure 4c) helps to provide structural information of the GO with different degree of reduction. Ferrari *et al.* have reported that the development of Raman D peak indicates disordering of graphite but ordering of amorphous carbon structures.[55] We believe the model provided by Ferrari *et al.* can be used to interpret our Raman results (Figure 4c). For very disordered structure, such as amorphous carbon or low mobility GO, the probability of finding a six-fold ring in the cluster is low and the intensity of the D band is related to the richness of the six-fold aromatic ring. Meanwhile, the G band is caused by in-plane bond stretching of pairs of sp^2 C atoms, and it occurs at all sp^2 sites and is not necessarily related to the presence of a six-fold ring. Therefore, I(D)/I(G) will increase with the mobility for the GO at low mobility regime (mobility <1 $cm^2/V \cdot s$). Once the GO is better reduced (more ordered), I(D)/I(G) will decrease with decreasing disorder in graphitic structures. Tuinstra and Koening (TK) have noted that I(D)/I(G) varies inversely with the crystallite size L_a in graphite:[56] $I(D)/I(G) = C(\lambda)/L_a$, where $C(\lambda)$ is the constant related to the excitation wavelength used in Raman. The TK relation is only valid when the 6 six-fold member rings are already present; hence, the relation can be used to estimate the crystallite size (graphitic domain size) for the reduced GO sheets with high mobility (>1 $cm^2/V \cdot s$) in our case), where the structure of reduced GO is closer to the graphene structure. Figure 5b shows that the estimated graphene nanocrystallite size (using TK relations) increases from 1 to ~4 nm when

the mobility is increased from 10 to 210 $cm^2/V \cdot s$, where the $C(\lambda)$ for a 488 nm laser is estimated to be 4.4 nm.[53,57]

Figure 4d shows that the ratio $I(2D)/I(G)$ of the reduced GO sheets increases slowly in the low mobility regime and faster in the high mobility regime. Both the G band downshift and the increase of the $I(2D)/I(G)$ ratio can be attributed to either (1) dedoping of p-type carriers in graphene[13,51,58] or (2) recovery of sp^2 C═C bonds (graphitization) in graphitic structures.[50] The $I(2D)/I(G)$ trend in Figure 4d is the same before and after DMF doping, although the Dirac point of these devices is greatly left-shifted, suggesting that the general observation for $I(2D)/I(G)$ is not governed by doping or dedoping here. Therefore, the graphitization appears to be a more appropriate explanation for the increase of $I(2D)/I(G)$, corroborating the conclusion from Figure 4c.

CONCLUSIONS

In summary, the GO sheets reduced by high-temperature alcohol vapors exhibit highly integrated graphitic structures and excellent electrical conductivity and carrier mobility. Raman spectroscopic studies reveal that the conductivity enhancement in the low mobility regime is attributed to the removal of chemical functional groups and the formation of six-fold rings. In the high mobility regime, the growth of the graphitic domain size becomes dominant in restoring its electrical conductivity. More investigations are required to further suppress the Raman D-band and promote the conductivity of GO sheets.

EXPERIMENTAL SECTION

Preparation of Graphene Oxide Sheets: Graphene oxide sheets were prepared by a modified Hummers' method from natural graphite flakes (NGS Naturgraphit GmbH, Germany).[36] In brief, 2 g of graphite flakes was mixed with concentrated H_2SO_4 (12 mL) and kept at 80 °C for 4.5 h. The solution was cooled to room temperature and then sonicated in a water bath (300 W; Finnsonic model 20) for 2 h. The sonication process is crucial for achieving desired large-sized GO flakes. The mixed solution was then diluted with 500 mL of deionized (DI) water and left overnight. The solution was filtered and washed using 200 nm porous filters to obtain the preoxidized graphite powders. The product was dried by gentle baking (70 °C), followed by drying. The preoxidized graphite powders were put into concentrated H_2SO_4 (120 mL), added with $KMnO_4$ (15 mg) in an ice bath, and stirred at room temperature for 2 h. The solution was diluted with DI water (250 mL), stirred for 2 h, and then added to 0.7 L of DI water. Shortly thereafter, 20 mL of H_2O_2 (30%) was added into the mixture, and the color changed to light yellow. After setting overnight, the top solution was collected (unreacted graphite powders were condensed at the bottom of the solution), then centrifuged (40 mL, 10 000 rpm) to obtain GO powders. To remove residual metal ions, these powders were dissolved in 1:10 HCl solution and then centrifuged. The processes were repeated at least three times. Finally, dissolution and centrifugation were performed in DI water to remove the unwanted acid.

Reduction Using Alcohol Vapors: Single-layer GO films were deposited onto the silicon substrates with 300 nm silicon oxide by the dip-coating method. These samples were loaded into a quartz tube, and forming gas (20% H_2 in Ar at 80−100 sccm) was introduced to the tube to purge undesired moisture and oxygen. The quartz tube was then heated to the desired temperature (600−1000 °C), followed by introducing absolute alcohol (EtOH) vapors into the tube using the forming gas (or pure Ar) as a carrier gas bubbling through an alcohol liquid maintained at 0 °C.

Preparation of Thin-Film Electrodes: Quartz substrates were first cleaned with a standard Piranha solution to remove undesired impurities. The slow and multiple dip-coating method was used to deposit GO sheets on quartz. Briefly, quartz substrates for receiving GO sheets were immersed in an aqueous GO suspension (0.062 mg/mL), followed by slow pulling (0.16 mm/s). The process was repeated for desired thickness of films. Then, the substrates were dried in air and followed by the alcohol reduction processes. The ultralarge reduced GO sheets can be used to prepare a conductive electrode with 98% transparency.

Fabrication of Field-Effect Transistor Devices: Single-layer GO films were deposited onto the silicon substrates with a 300 nm silicon oxide layer by the dip-coating method, followed by alcohol reduction. The dip-coating condition was tuned to deposit loosely distributed GO sheets on substrates. It is noted that most of the deposited GO sheets are monolayered. The field-effect transistor device was fabricated by evaporating Au electrodes (40 nm thick) directly on top of the selected, regularly shaped reduced GO sheets using a copper grid (200 mesh, 20 μm spacing) as a hardmask. The typically obtained channel length between source and drain electrodes was around 20 μm. The dimethylformamide (DMF) vapor soaking was performed by putting the device in a sealed vessel together with a small drop of DMF for 8 h.

Characterizations and Electrical Measurements: Sheet resistance was measured using the four point probe method (Keithley Instrument), and the transmittance measurement was done with a UV−vis−NIR spectrophotometer (Perkin-Elmer). The Raman spectra were measured in a WITec CRM300 confocal Raman microscopy system (with a laser wavelength of 488 nm and laser spot size of ~0.5 μm), and the Si peak at 520 cm^{-1} was used as a reference for wavenumber calibration. All electrical measurements were performed under ambient conditions using a Keithley semiconductor parameter analyzer, model 4200-SCS. XPS measurements were carried out by a Kratos AXIS-ultra spectrometer (UK) with monochromatic Al Kα X-ray radiation (1486.71 eV).

Acknowledgment. This research was mainly supported by Research Center for Applied Science, Academia Sinica (Nano program) and Natinoal Science Council Taiwan (NSC-99-2112-M-001-021-MY3 and 99-2738-M-001-001). We also thank part of the financial support from National Research Foundation Singapore (NRF-CRP2-2007-02). We thank the useful discussions with Prof. Laurie E. Mcneil (Department of Physics & Astronomy, University of North Carolina at Chapel Hill).

Supporting Information Available: Raman spectra, electrical data, AFM images, and SEM photos are included. This material is available free of charge *via* the Internet at http://pubs.acs.org.

REFERENCES AND NOTES

1. Novoselov, K. S.; Geim, A. K.; Morozov, S. V.; Jiang, D.; Zhang, Y.; Dubonos, S. V.; Grigorieva, I. V.; Firsov, A. A. Electric Field Effect in Atomically Thin Carbon Films. *Science* **2004**, *306*, 666–669.
2. Novoselov, K. S.; Geim, A. K.; Morozov, S. V.; Jiang, D.; Katsnelson, M. I.; Grigorieva, I. V.; Dubonos, S. V.; Firsov, A. A. Two-Dimensional Gas of Massless Dirac Fermions in Graphene. *Nature* **2005**, *438*, 197–200.
3. Novoselov, K. S.; Jiang, D.; Schedin, F.; Booth, T. J.;

Khotkevich, V. V.; Morozov, S. V.; Geim, A. K. Two-Dimensional Atomic Crystals. *Proc. Natl. Acad. Sci. U.S.A.* **2005**, *102*, 10451–10453.
4. Bolotin, K. I.; Sikes, K. J.; Jiang, Z.; Klima, M.; Fudenberg, G.; Hone, J.; Kim, P.; Stormer, H. L. Ultrahigh Electron Mobility in Suspended Graphene. *Solid State Commun.* **2008**, *146*, 351–355.
5. Zhang, Y.; Tan, Y.-W.; Stormer, H. L.; Kim, P. Experimental Observation of the Quantum Hall Effect and Berry's Phase in Graphene. *Nature* **2005**, *438*, 201–204.
6. Han, M. Y.; Ozyilmaz, B.; Zhang, Y.; Kim, P. Energy Band-Gap Engineering of Graphene Nanoribbons. *Phys. Rev. Lett.* **2007**, *98*, 206805-4.
7. Zhang, Y.; Tang, T.-T.; Girit, C.; Hao, Z.; Martin, M. C.; Zettl, A.; Crommie, M. F.; Shen, Y. R.; Wang, F. Direct Observation of a Widely Tunable Bandgap in Bilayer Graphene. *Nature* **2009**, *459*, 820–823.
8. Lee, C.; Wei, X.; Kysar, J. W.; Hone, J. Measurement of the Elastic Properties and Intrinsic Strength of Monolayer Graphene. *Science* **2008**, *321*, 385–388.
9. Balandin, A. A.; Ghosh, S.; Bao, W.; Calizo, I.; Teweldebrhan, D.; Miao, F.; Lau, C. N. Superior Thermal Conductivity of Single-Layer Graphene. *Nano Lett.* **2008**, *8*, 902–907.
10. Chen, Z.; Lin, Y.-M.; Rooks, M. J.; Avouris, P. Graphene Nano-Ribbon Electronics. *Physica E* **2007**, *40*, 228–232.
11. Lemme, M. C.; Echtermeyer, T. J.; Baus, M.; Kurz, H. A Graphene Field-Effect Device. *IEEE Electron Device Lett.* **2007**, *28*, 282–284.
12. Martin, J.; Akerman, N.; Ulbricht, G.; Lohmann, T.; Smet, J. H.; von Klitzing, K.; Yacoby, A. Observation of Electron-Hole Puddles in Graphene Using a Scanning Single-Electron Transistor. *Nat. Phys.* **2008**, *4*, 144–148.
13. Das, A; Pisana, S; Chakraborty, B; Piscanec, S; Saha, S. K.; Waghmare, U. V.; Novoselov, K. S.; Krishnamurthy, H. R.; Geim, A. K.; Ferrari, A. C.; *et al.* Monitoring Dopants by Raman Scattering in an Electrochemically Top-Gated Graphene Transistor. *Nat. Nanotechnol.* **2008**, *3*, 210–215.
14. Eda, G.; Fanchini, G.; Chhowalla, M. Large-Area Ultrathin Films of Reduced Graphene Oxide as a Transparent and Flexible Electronic Material. *Nat. Nanotechnol.* **2008**, *3*, 270–274.
15. Tung, V. C.; Chen, L.-M.; Allen, M. J.; Wassei, J. K.; Nelson, K.; Kaner, R. B.; Yang, Y. Low-Temperature Solution Processing of Graphene-Carbon Nanotube Hybrid Materials for High-Performance Transparent Conductors. *Nano Lett.* **2009**, *9*, 1949–1955.
16. Becerril, H. A.; Mao, J.; Liu, Z.; Stoltenberg, R. M.; Bao, Z.; Chen, Y. Evaluation of Solution-Processed Reduced Graphene Oxide Films as Transparent Conductors. *ACS Nano* **2008**, *2*, 463–470.
17. Matyba, P.; Yamaguchi, H.; Eda, G.; Chhowalla, M.; Edman, L.; Robinson, N. D. Graphene and Mobile Ions: The Key to All-Plastic, Solution-Processed Light-Emitting Devices. *ACS Nano* **2010**, *4*, 637–642.
18. Stankovich, S.; Dikin, D. A.; Dommett, G. H. B.; Kohlhaas, K. M.; Zimney, E. J.; Stach, E. A.; Piner, R. D.; Nguyen, S. T.; Ruoff, R. S. Graphene-Based Composite Materials. *Nature* **2006**, *442*, 282–286.
19. Yoo, E.; Kim, J.; Hosono, E.; Zhou, H.-S.; Kudo, T.; Honma, I. Large Reversible Li Storage of Graphene Nanosheet Families for Use in Rechargeable Lithium Ion Batteries. *Nano Lett.* **2008**, *8*, 2277–2282.
20. Dong, X. C.; Shi, Y. M.; Huang, W.; Chen, P.; Li, L. J. Electrical Detection of DNA Hybridization with Single-Base Specificity Using Transistors Based on CVD-Grown Graphene Sheets. *Adv. Mater.* **2010**, *22*, 1649–1653.
21. Hu, W.; Peng, C.; Luo, W.; Lv, M.; Li, X.; Li, D.; Huang, Q.; Fan, C. Graphene-Based Antibacterial Paper. *ACS Nano* **2010**, *4*, 4317–4323.
22. Mohanty, N.; Berry, V. Graphene-Based Single-Bacterium Resolution Biodevice and DNA Transistor: Interfacing Graphene Derivatives with Nanoscale and Microscale Biocomponents. *Nano Lett.* **2008**, *8*, 4469–4476.
23. He, Q.; Sudibya, H. G.; Yin, Z.; Wu, S.; Li, H.; Boey, F.; Huang, W.; Chen, P.; Zhang, H. Centimeter-Long and Large-Scale Micropatterns of Reduced Graphene Oxide Films: Fabrication and Sensing Applications. *ACS Nano* **2010**, *4*, 3201–3208.
24. Berger, C.; Song, Z.; Li, X.; Wu, X.; Brown, N.; Naud, C.; Mayou, D.; Li, T.; Hass, J.; Marchenkov, A. N.; *et al.* Electronic Confinement and Coherence in Patterned Epitaxial Graphene. *Science* **2006**, *312*, 1191–1196.
25. Sutter, P. W.; Flege, J.-I.; Sutter, E. A. Epitaxial Graphene on Ruthenium. *Nat. Mater.* **2008**, *7*, 406–411.
26. Liang, X.; Fu, Z.; Chou, S. Y. Graphene Transistors Fabricated *via* Transfer-Printing in Device Active-Areas on Large Wafer. *Nano Lett.* **2007**, *7*, 3840–3844.
27. Reina, A.; Jia, X.; Ho, J.; Nezich, D.; Son, H.; Bulovic, V.; Dresselhaus, M. S.; Kong, J. Large Area, Few-Layer Graphene Films on Arbitrary Substrates by Chemical Vapor Deposition. *Nano Lett.* **2009**, *9*, 30–35.
28. Li, X.; Cai, W.; An, J.; Kim, S.; Nah, J.; Yang, D.; Piner, R.; Velamakanni, A.; Jung, I.; Tutuc, E.; *et al.* Large-Area Synthesis of High-Quality and Uniform Graphene Films on Copper Foils. *Science* **2009**, *324*, 1312–1314.
29. Stankovich, S.; Dikin, D. A.; Piner, R. D.; Kohlhaas, K. A.; Kleinhammes, A.; Jia, Y.; Wu, Y.; Nguyen, S. T.; Ruoff, R. S. Synthesis of Graphene-Based Nanosheets *via* Chemical Reduction of Exfoliated Graphite Oxide. *Carbon* **2007**, *45*, 1558–1565.
30. Park, S.; Ruoff, R. S. Chemical Methods for The Production of Graphenes. *Nat. Nanotechnol.* **2009**, *4*, 217–224.
31. Park, S.; An, J.; Jung, I.; Piner, R. D.; An, S. J.; Li, X.; Velamakanni, A.; Ruoff, R. S. Colloidal Suspensions of Highly Reduced Graphene Oxide in a Wide Variety of Organic Solvents. *Nano Lett.* **2009**, *9*, 1593–1597.
32. Luo, Z.; Lu, Y.; Somers, L. A.; Johnson, A. T. C. High Yield Preparation of Macroscopic Graphene Oxide Membranes. *J. Am. Chem. Soc.* **2009**, *131*, 898–899.
33. Gomez-Navarro, C.; Weitz, R. T.; Bittner, A. M.; Scolari, M.; Mews, A.; Burghard, M.; Kern, K. Electronic Transport Properties of Individual Chemically Reduced Graphene Oxide Sheets. *Nano Lett.* **2009**, *9*, 2206.
34. Williams, G.; Seger, B.; Kamat, P. V. TiO_2-Graphene Nanocomposites. UV-Assisted Photocatalytic Reduction of Graphene Oxide. *ACS Nano* **2008**, *2*, 1487–1491.
35. Hummers, W. S.; Offeman, R. E. Preparation of Graphitic Oxide. *J. Am. Chem. Soc.* **1958**, *80*, 1339.
36. Su, C.-Y.; Xu, Y.; Zhang, W.; Zhao, J.; Tang, X.; Tsai, C.-H.; Li, L.-J. Electrical and Spectroscopic Characterizations of Ultra-Large Reduced Graphene Oxide Monolayers. *Chem. Mater.* **2009**, *21*, 5674–5680.
37. Cote, L. J.; Kim, F.; Huang, J. Langmuir-Blodgett Assembly of Graphite Oxide Single Layers. *J. Am. Chem. Soc.* **2009**, *131*, 1043–1049.
38. Li, D.; Muller, M. B.; Gilje, S.; Kaner, R. B.; Wallace, G. G. Processable Aqueous Dispersions of Graphene Nanosheets. *Nat. Nanotechnol.* **2008**, *3*, 101–105.
39. Li, X.; Wang, H.; Robinson, J. T.; Sanchez, H.; Diankov, G.; Dai, H. Simultaneous Nitrogen Doping and Reduction of Graphene Oxide. *J. Am. Chem. Soc.* **2009**, *131*, 15939–15944.
40. López, V.; Sundaram, R. S.; Gómez-Navarro, C.; Olea, D.; Burghard, M.; Gómez-Herrero, J.; Zamora, F.; Kern, K. Chemical Vapor Deposition Repair of Graphene Oxide: A Route to Highly-Conductive Graphene Monolayers. *Adv. Mater.* **2009**, *21*, 4683–4686.
41. Gao, W.; Alemany, L. B.; Ci, L.; Ajayan, P. M. New Insights into the Structure and Reduction of Graphite Oxide. *Nat. Chem.* **2009**, *1*, 403–408.
42. Wu, J.; Becerril, H. A.; Bao, Z.; Liu, Z.; Chen, Y.; Peumans, P. Organic Solar Cells with Solution-Processed Graphene Transparent Electrodes. *Appl. Phys. Lett.* **2008**, *92*, 263302-1.
43. Wu, X.; Sprinkle, M.; Li, X.; Ming, F.; Berger, C.; de Heer, W. A. Epitaxial-Graphene/Graphene-Oxide Junction: An Essential Step towards Epitaxial Graphene Electronics. *Phys. Rev. Lett.* **2008**, *101*, 026801-1.
44. Stankovich, S.; Piner, R. D.; Chen, X.; Wu, N.; Nguyen, S. T.;

Ruoff, R. S. Stable Aqueous Dispersions of Graphitic Nanoplatelets *via* the Reduction of Exfoliated Graphite Oxide in the Presence of Poly(sodium 4-styrenesulfonate). *J. Mater. Chem.* **2006**, *16*, 155–158.
45. Xu, Y.; Bai, H.; Lu, G.; Li, C.; Shi, G. Flexible Graphene Films *via* the Filtration of Water-Soluble Noncovalent Functionalized Graphene Sheets. *J. Am. Chem. Soc.* **2008**, *130*, 5856–5857.
46. Maruyama, S.; Kojima, R.; Miyauchi, Y.; Chiashi, S.; Kohno, M. Low-Temperature Synthesis of High-Purity Single-Walled Carbon Nanotubes from Alcohol. *Chem. Phys. Lett.* **2002**, *360*, 229–234.
47. Gupta, A.; Chen, G.; Joshi, P.; Tadigadapa, S.; Eklund, P. C. Raman Scattering from High-Frequency Phonons in Supported n-Graphene Layer Films. *Nano Lett.* **2006**, *6*, 2667–2673.
48. Ferrari, A. C.; Meyer, J. C.; Scardaci, V.; Casiraghi, C.; Lazzeri, M.; Mauri, F.; Piscanec, S.; Jiang, D.; Novoselov, K. S.; Roth, S.; *et al.* Raman Spectrum of Graphene and Graphene Layers. *Phys. Rev. Lett.* **2006**, *97*, 187401-1.
49. Graf, D.; Molitor, F.; Ensslin, K.; Stampfer, C.; Jungen, A.; Hierold, C.; Wirtz, L. Spatially Resolved Raman Spectroscopy of Single- and Few-Layer Graphene. *Nano Lett.* **2007**, *7*, 238–242.
50. Krauss, B.; Lohmann, T.; Chae, D. H.; Haluska, M.; von Klitzing, K.; Smet, J. H. Laser-Induced Disassembly of a Graphene Single Crystal into a Nanocrystalline Network. *Phys. Rev. B.* **2009**, *79*, 165428-1.
51. Dong, X. C.; Fu, D. C.; Fang, W. J.; Shi, Y. M.; Cheng, P.; Li, L. J. Doping Single-Layer Graphene with Aromatic Molecules. *Small* **2009**, *5*, 1422–1426.
52. Chieu, T. C.; Dresselhaus, M. S.; Endo, M. Raman Studies of Benzene-Derived Graphite Fibers. *Phys. Rev. B* **1982**, *26*, 5867–5877.
53. Ferrari, A. C. Raman Spectroscopy of Graphene and Graphite: Disorder, Electron-Phonon Coupling, Doping and Nonadiabatic Effects. *Solid State Commun.* **2007**, *143*, 47–57.
54. Pimenta, M. A.; Dresselhaus, G.; Dresselhaus, M. S.; Cancado, L. G.; Jorio, A.; Saito, R. Studying Disorder in Graphite-Based Systems by Raman Spectroscopy. *Phys. Chem. Chem. Phys.* **2007**, *9*, 1276–1291.
55. Ferrari, A. C.; Robertson, J. Interpretation of Raman Spectra of Disordered and Amorphous Carbon. *Phys. Rev. B* **2000**, *61*, 14095–14107.
56. Tuinstra, F.; Koenig, J. L. Raman Spectrum of Graphite. *J. Chem. Phys.* **1970**, *53*, 1126–1130.
57. Matthews, M. J.; Pimenta, M. A.; Dresselhaus, G.; Dresselhaus, M. S.; Endo, M. Origin of Dispersive Effects of the Raman D Band in Carbon Materials. *Phys. Rev. B.* **1999**, *59*, R6585–R6588.
58. Yan, J.; Zhang, Y.; Kim, P.; Pinczuk, A. Electric Field Effect Tuning of Electron-Phonon Coupling in Graphene. *Phys. Rev. Lett.* **2007**, *98*, 166802-1.